J Solid State Electrochem (2009) 13:1497–1504
DOI 10.1007/s10008-009-0880-8

ORIGINAL PAPER

A joint electrochemical/spectroelectrochemical inspection (and re-inspection) of high-nuclearity platinum carbonyl clusters

Serena Fedi · Piero Zanello · Franco Laschi · Alessandro Ceriotti · Simona El Afefey

Received: 13 February 2009 / Revised: 25 May 2009 / Accepted: 2 June 2009 / Published online: 23 June 2009
© Springer-Verlag 2009

Abstract The accurate study of the electron transfer activity of the tetraanion $[Pt_{19}(CO)_{22}]^{4-}$ is presented together with that of the dianion $[Pt_{38}(CO)_{44}]^{2-}$, which was previously studied by spectroelectrochemistry but only partially examined from the electrochemical viewpoint. The main feature of the two clusters is that they undergo a sequence of close-spaced pairs of reversible one-electron processes, which are qualitatively reminiscent of those exhibited by the dianion $[Pt_{24}(CO)_{30}]^{2-}$. In order to focus on such unique aspect of the three structurally characterised platinum clusters, we have investigated (and reinvestigated) their electrochemical and spectroelectrochemical redox properties, also reporting on the electron paramagnetic resonance (EPR) spectrum of the monoanion $[Pt_{24}(CO)_{30}]^{-}$, which represents the first successful study of the paramagnetism of homoleptic platinum–carbonyl clusters.

Keywords Metal clusters · Electron transfer activity · Spectroelectrochemistry

S. Fedi · P. Zanello (✉) · F. Laschi
Dipartimento di Chimica, University of Siena,
Via A. De Gasperi, 2,
53100 Siena, Italy
e-mail: zanello@unisi.it

A. Ceriotti · S. El Afefey
Dipartimento di Chimica Inorganica,
Metallorganica e Analitica "Lamberto Malatesta",
University of Milan,
Via, Venezian 21,
20133 Milan, Italy

A. Ceriotti
e-mail: alessandro.ceriotti@unimi.it

Introduction

Metal clusters having a metallic core contained in a ligand shell could be valid candidates as components of data storage devices and could potentially represent the ultimate solution for miniaturisation in nanoelectronics [1–8]. As a matter of fact, metal–carbonyl clusters can be considered in principle as microscopic capacitors in that they are constituted by a kernel of metal atoms surrounded by a shell of nominally insulating carbonyl ligands. Nevertheless, such a morphological similarity must be accompanied by a series of further requirements, such as: (1) electron-sink behaviour, i.e. they should be able to accept and release electrons reversibly (or they must maintain unaltered their original molecular structure); (2) effective insulation of the metallic core from the carbonyl shell able to hamper the intermolecular exchange of electrons. In fact, easy intermolecular electron exchanges prevent the effective storage of electrons in the molecule. In this connection, evidences of the ability of metal cores of high nuclearity metal–carbonyl clusters to act as a quantum dot have been gained [9]; (3) finally, for practical purposes, the metallic core should display dimensions falling in the nanometric field in order to have the possibility to interact with a single molecule, rather than with a collection of molecules [7].

In this picture, the analysis of the redox properties of metal–carbonyl clusters is of primary importance to establish their stability and their electron-sink behaviour, which implies their ability to give rise to sequences of reversible redox processes or to possess a HOMO–LUMO frontier region in which one or more orbitals weakly antibonding or non-bonding can be populated or de-populated without great effects on the metal framework stability [10].

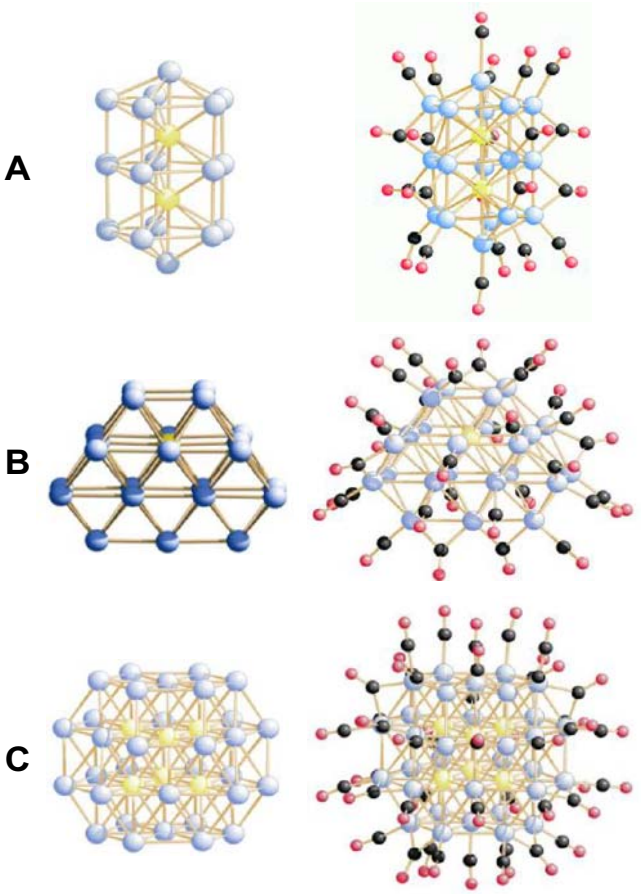

Fig. 1 X-Ray structures, together with the metal core composition, of : **A** $[Pt_{19}(CO)_{22}]^{4-}$; **B** $[Pt_{24}(CO)_{30}]^{2-}$; **C** $[Pt_{38}(CO)_{44}]^{2-}$

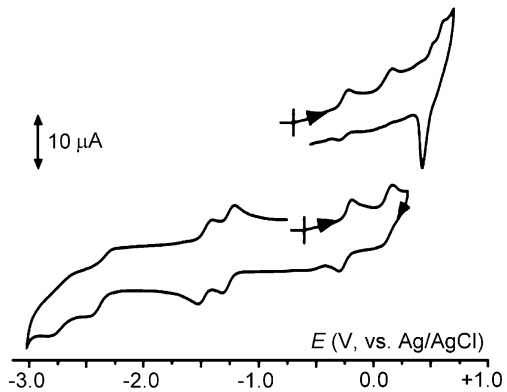

Fig. 2 Cyclic voltammetric responses recorded at a glassy carbon electrode in DMF solution of $[Pt_{19}(CO)_{22}]^{4-}$ ($1.0\ 10^{-3}$ mol dm^{-3}). $[NEt_4][PF_6]$ supporting electrolyte (0.1 mol dm^{-3}). Scan rate 0.2 V s^{-1}. T= 293 K

Table 1 Formal electrode potentials [V, vs. Ag/AgCl and (in brackets) vs. Fc/Fc^+] for the redox changes exhibited by $[Pt_{19}(CO)_{22}]^{4-}$ in different solvents and at different temperatures

Oxidation processes				Reduction processes				Solvent	Temperature (K)
$E_c^{\theta'}$ (0/–)	$E_c^{\theta'}$ (–/2–)	$E_c^{\theta'}$ (2–/3–)	$E_c^{\theta'}$ (3–/4–)	$E_c^{\theta'}$ (4–/5–)	$E_c^{\theta'}$ (5–/6–)	$E_c^{\theta'}$ (6–7–)	$E_c^{\theta'}$ (7–/8–)		
+0.51[a] (+0.09)[a]	+0.43[a] (+0.01)[a]	+0.12[a] (–0.32)[a]	–0.15 (–0.57)	–1.13 (–1.55)	–1.22 (–1.64)	–2.03 (–2.45)	–2.20 (–2.62)	MeCN	278
+052[a] (+0.10)[a]	+0.44[a] (+0.00)[a]	+0.11[a] (–0.31)[a]	–0.20 (–0.62)	–1.10 (–1.52)	–1.27 (–1.69)	–2.12 (–2.54)	–2.29 (–2.71)		298
+0.62[a] (+0.08)[a]	+0.53[a] (+0.10)[a]	+0.18[a] (–0.26)[a]	–0.24 (–0.68)	–1.25 (–1.68)	–1.45 (–1.89)	–2.38 (–2.82)	–2.70 (–3.14)	DMF	278
–	+0.59[a] (+0.15)[a]	+0.14[a] (–0.30)[a]	–0.30 –0.74	–1.25 (–1.69)	–1.50 (–1.94)	–2.37 (–2.81)	–2.68 (–3.12)		298

[a] Peak potential value for irreversible processes.

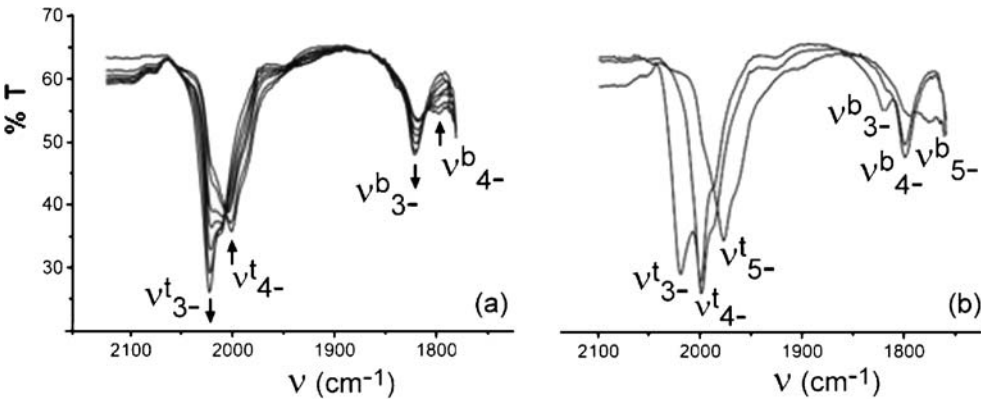

Fig. 3 Infrared spectral changes recorded in an OTTLE cell upon: **a** progressive one-electron oxidation of $[Pt_{19}(CO)_{22}]^{4-}$; **b** overall changes 3−/4−/5−. DMF solution; $[NBu_4][PF_6]$ as supporting electrolyte (0.1 mol dm^{-3})

In this picture, we deal with an accurate electrochemical investigation (going in some cases in more depth with previous studies [11–13]) of the structurally characterised, high-nuclearity, platinum clusters $[Pt_{19}(CO)_{22}]^{4-}$ [14], $[Pt_{24}(CO)_{30}]^{2-}$ [13] and $[Pt_{38}(CO)_{44}]^{2-}$ [13, 15], the structures of which are schematically shown in Fig. 1.

Experimental section

The platinum carbonyl clusters have been prepared according to literature references [13–15]. Anhydrous 99.8% acetonitrile, 99.8% *N*,*N* dimethylformamide (DMF), and dichloromethane 99.8% were Aldrich products. Anhydrous 99.9% HPLC-grade tetrahydrofuran (Aldrich) was distilled in the presence of sodium before use. Fluka $[NBu_4][PF_6]$ and $[NEt_4][PF_6]$ (electrochemical grade) were used as supporting electrolytes. Cyclic voltammetry was performed in a three-electrode cell containing the working electrode surrounded by a platinum-spiral counter electrode and the reference electrode (Ag/AgCl) mounted with a Luggin capillary. Platinum or gold or glassy-carbon electrodes were used as working electrodes. For low-temperature measurements, a non-isothermal assembly was set up in which the central part of the cell was enclosed by a thermostatic jacket through which a cooled liquid was circulated.

Controlled potential coulometry was performed in an H-shaped cell with anodic and cathodic compartments separated by a sintered-glass disk. The working macroelectrode was a platinum gauze; a mercury pool was used as the counter electrode.

A BAS 100 W electrochemical analyser was used as the polarising unit.

All the potential values have been measured with respect to the Ag/AgCl reference electrode. Under the present experimental conditions, at 293 K, the one-electron oxidation of ferrocene occurs at $E_c^{\theta,} = +0.42$ V in acetonitrile, at $E_c^{\theta,} = +0.44\ V$ in dimethylformamide, at $E_c^{\theta,} = +0.43$ V in dichloromethane, and at $E_c^{\theta,} = +0.49$ V in tetrahydrofuran solutions.

UV–vis and infra-red (IR) spectroelectrochemical measurements were carried out using Perkin-Elmer Lambda 900 UV–vis and FT-IR System SPECTRUM BX spectrophotometers, respectively, and an optically transparent thin-layer electrode cell (OTTLE cell) equipped with a Pt-minigrid working electrode (32 wires/cm), Pt minigrid auxiliary electrode, Ag wire pseudoreference and CaF_2 windows [16]. During the microelectrolysis procedures, the electrode potential was controlled by an Amel potentiostat 2059 equipped with an Amel function generator 568.

Electron spin resonance spectra were recorded with an ER 200 D-SRC Bruker spectrometer operating at X-band frequencies using a HS Bruker rectangular cavity. The control of the operational frequency was obtained with a

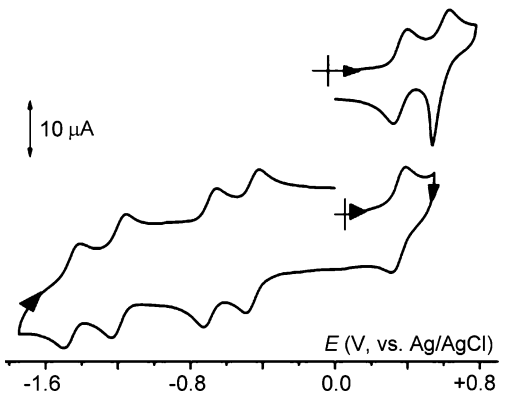

Fig. 4 Cyclic voltammetric responses recorded at a glassy carbon electrode in CH_2Cl_2 solution of $[Pt_{24}(CO)_{30}]^{2-}$ (0.5 10^{-3} mol dm^{-3}). $[NBu_4][PF_6]$ supporting electrolyte (0.2 mol dm^{-3}). Scan rate 0.2 V s^{-1}. T=298 K

Table 2 Formal electrode potentials [V, vs. Ag/AgCl and (in brackets) vs. Fc/Fc^+] for the electron transfer processes exhibited by $[Pt_{24}(CO)_{30}]^{2-}$ in different solvents, at different temperatures

Oxidation processes		Reduction processes				Solvent	Temperature (K)
$E_c^{\theta'}$ (−/0)	$E_c^{\theta'}$ (2−/−)	$E_c^{\theta'}$ (2−/3−)	$E_c^{\theta'}$ (3−/4−)	$E_c^{\theta'}$ (4−/5−)	$E_c^{\theta'}$ (5−/6−)		
+0.64[a] (+0.21)[a]	+0.36 (−0.07)	−0.45 (−0.88)	−0.68 (−1.11)	−1.18 (−1.61)	−1.44 (−1.87)	CH_2Cl_2	278
+0.64[a] (+0.21)[a]	+0.34 (−0.09)	−0.47 (−0.90)	−0.72 (−1.15)	−1.22 (−1.65)	−1.48 (−1.91)		298
+0.69[b] (+0.4)[c]	+0.44[b] (+0.15)[c]	−0.38[b] (−0.7)[c]	−0.64[b] (−1.0)[c]	−1.13[b] (−1.45)[c]	−1.39[b] (−1.7)[c]		298
+0.98[a] (+0.49)[a]	+0.58 (+0.16)	−0.30 (−0.79)	−0.65 (−1.14)	−1.20 (−1.63)	−1.45 (−1.94)	THF	278
+0.98[a] (+0.49)[a]	+0.65 (+0.12)	−0.33 (−0.82)	−0.68 (−1.17)	−1.22 (−1.71)	−1.46 (−1.95)		298
	(+0.7)[c]	(−0.2)[c]	(−0.65)[c]	(−1.1)[c]	(−1.4)[c]		298

[a] Peak potential value for processes complicated by adsorption phenomena (see text)

[b] From [12]

[c] From [13] (approximate values from spectroelectrochemical tests)

Hewlett-Packard X 5-32 B wavemeter, and the magnetic field was calibrated with a 1,1-diphenyl-2-picrylhydrazyl (DPPH) radical as a suitable field marker. The *g* values are referred to DPPH (g=2.0036) used as an external standard reference.

Results and discussion

$[Pt_{19}(CO)_{22}]^{4-}$

As illustrated in Fig. 2, the redox activity of the $[NBu_4]$ salt of the tetra-anion $[Pt_{19}(CO)_{22}]^{4-}$ can be represented as two pairs of anodic processes and two pairs of cathodic processes, the members of each pair manifesting in most cases features of chemical reversibility.

Controlled potential coulometric tests in correspondence of the first oxidation (E_w=−0.2 V) proved that it involves one electron *per* molecule. Cyclic voltammetry on the exhaustively oxidised solution affords responses quite complementary to the original one, thus indicating the complete stability of the trianion $[Pt_{19}(CO)_{22}]^{3-}$.

Analysis of the cyclic voltammograms of either the first oxidation or the two first reductions with scan rates progressively increasing from 0.02 to 2.00 V s^{-1} confirmed the occurrence of simple one-electron processes. In fact, in all cases: (1) the current ratio $i_{p(reverse)}/i_{p(forward)}$ is constantly equal to 1.0; (2) the current function $i_{p(forward)}/v^{1/2}$

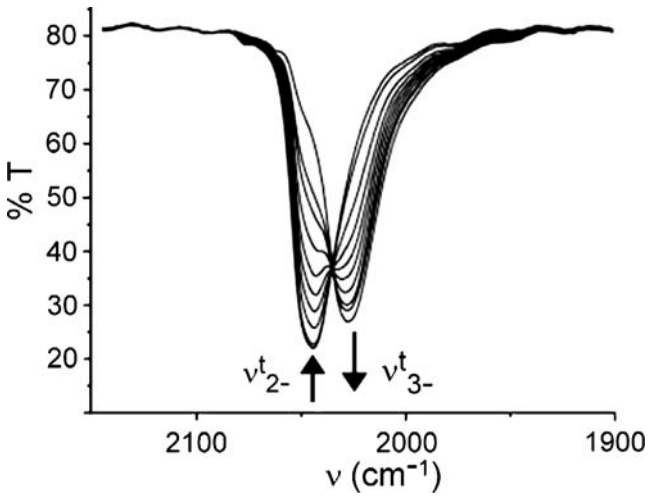

Fig. 5 IR spectral changes recorded in an OTTLE cell upon the progressive reduction $[Pt_{24}(CO)_{30}]^{2-/3-}$. CH_2Cl_2 solution; $[NBu_4][PF_6]$ supporting electrolyte (0.2 mol dm^{-3})

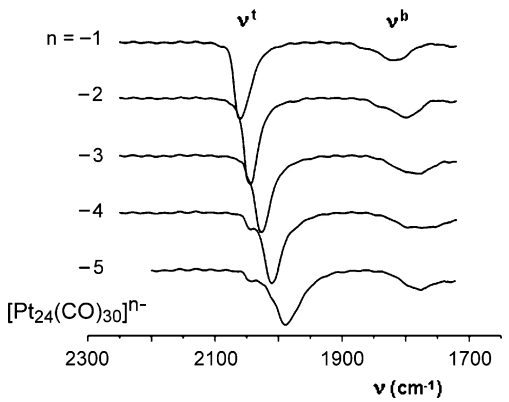

Fig. 6 Selected IR spectra recorded in an OTTLE cell as a function of the charge of the cluster $[Pt_{24}(CO)_{30}]^{n-}$. CH_2Cl_2 solution; $[NBu_4][PF_6]$ supporting electrolyte (0.2 mol dm^{-3})

Table 3 IR stretching frequencies (cm^{-1}) of the terminal (ν^t) and bridging (ν^b) carbonyl groups for the series $[Pt_{24}(CO)_{30}]^{n-}$. CH_2Cl_2 solution

"n" cluster charge	ν^t_{CO}		ν^b_{CO}	
1−	2,060	1,870	1,850	1,820
	2,061[a]	1,875[a]	1,825[a]	1,818[a]
2−	2,043	1,840	1,798	
	2,045[a]	1,835[a]	1,800[a]	
3−	2,027	1,798	1,779	
	2,028[a]	1,795[a]		
4−	2,008	1,797	1,773	
	2,010[a]	1,780[a]		
5−	1,990	1,775		
	1,991[a]	1,766[a]		

[a] From [13]

remains essentially constant; (3) the peak-to-peak separation does not depart appreciably from the theoretical value of 57 mV [17].

As shown, the two most anodic processes show in the backscan an adsorption peak likely due to the neutral species $[Pt_{19}(CO)_{22}]^0$.

The redox potentials of the cited electron transfer processes either at different temperatures or in different solvents are summarised in Table 1.

The decrease of the temperature from 298 to 258 K does not appreciably modify the voltammetric picture. As far as the role of the solvent is concerned, the DMF solvation looks like it is to exert a shielding effect towards the electron addition processes higher than that exerted by MeCN.

Since the stretching vibrations of the carbonyl groups constitute a sensitive probe of its metal-to-carbon back-donation, we followed by IR spectroelectrochemistry how the ν_{CO} of both the terminal and the bridging groups of $[Pt_{19}(CO)_{22}]^{4-}$ vary during the easily accessible redox changes 4−/3− and 4−/5−, respectively.

In both cases, the spectral trend put in evidence the appearance of isosbestic points confirming the stability of all the cited oxidation states. Figure 3a representatively illustrates the IR spectral trend recorded in the 4−/3− passage.

The original spectrum shows two main absorptions at 2,001 cm^{-1}, which is assigned to the stretching vibration of the carbonyl groups terminally bounded at the metal core $\left(\nu^t_{4-}\right)$, and at 1,801 cm^{-1}, which is assigned to the stretching vibration of the bridged carbonyl groups $\left(\nu^b_{4-}\right)$, respectively. Upon oxidation, the two bands undergo an upshift at $2,020\ cm^{-1}\left(\nu^t_{3-}\right)$ and $1,820\ cm^{-1}\left(\nu^b_{3-}\right)$, respectively, suggesting a decrease of the dπ-Pt→π*-CO back-bonding.

In turn, as illustrated in Fig. 3b, upon reduction, the stretching vibrations of the terminal and bridging carbonyl groups undergo a downshift [1,960 cm^{-1} (ν^t_{5-}) and 1,740 cm^{-1}($\nu_{5-}{}^b$)] indicating an increase of the back-donation.

$[Pt_{24}(CO)_{30}]^{2-}$

As illustrated in Fig. 4, the $[PPh_4]$ salt of the dianion $[Pt_{24}(CO)_{30}]^{2-}$ also exhibits a rich redox activity [12, 13], in that it undergoes a pair of coulometrically measured one-electron oxidations and two pairs of one-electron reductions, all having features of chemical reversibility. The most anodic oxidation step, also in this case, is affected by electrode adsorption of the neutral species $[Pt_{24}(CO)_{30}]^0$.

The pertinent redox potentials are compiled in Table 2, also in comparison with those from previous investigations [12, 13]. Some differences hold likely due to the different supporting electrolytes, but especially because in [13] the formal electrode potentials have been indirectly deduced from spectrolectrochemical tests (thus introducing some significant margins of uncertainty). It is noted that no appreciable difference exist between dichloromethane and tetrahydrofuran as far as the redox potential of the different redox changes are concerned.

As representatively illustrated in Fig. 5, the spectroelectrochemical trend for the reduction step $[Pt_{24}(CO)_{30}]^{2-/3-}$

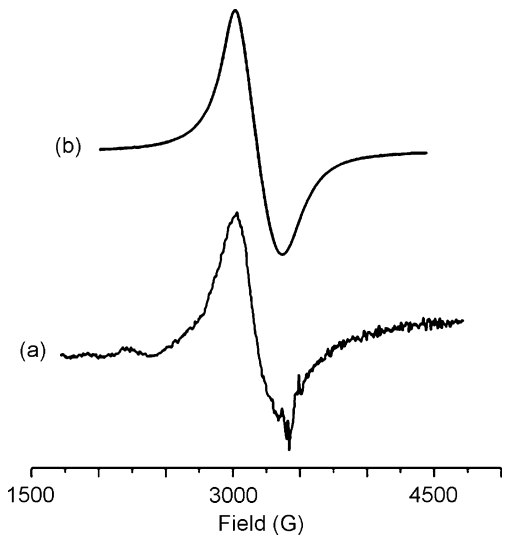

Fig. 7 X-band EPR spectrum of the monoanion $[Pt_{24}(CO)_{30}]^-$ electrogenerated in CH_2Cl_2 solution. Experimental (*a*) and simulated (*b*) lineshapes. T=100 K; ν=9.448 Ghz

Table 4 X-band simulated EPR spectral parameters of $[Pt_{24}(CO)_{30}]^{-}$

g_l	g_m	g_h	<g>	δg_{l-h}	a_l	a_m	a_h	<a>	ΔH_l	ΔH_m	ΔH_h	<ΔH>
2.210	2.120	2.020	2.117	0.190	40	80	60	60	110	65	130	102
					70	50	30	50	110	65	130	102

T=100 K. g_i, $\delta g_{l-h}=g_l-g_h$, $<g>=(g_l+g_m+g_h)/3$: ±0.008; a_i, $<a>=(a_l+a_m+a_h)/3$: ±8 G; ΔH_i, $<\Delta H>=(\Delta H_l+\Delta H_m+\Delta H_h)/3$: ±10 G. ν= 9.448 GHz.

displays an isosbestic point at 2,034 cm^{-1}, which confirms the stability of the two oxidation states.

Figure 6 gives the overall picture of the most significant IR spectroelectrochemical changes recorded as a function of the sequence of stepwise redox processes $[Pt_{24}(CO)_{30}]^{1-/2-/3-/4-/5-}$.

In agreement with previous findings [13], the stretching vibrations of the terminal carbonyl groups (ν^t) exhibit a linear downshift of 17–18 cm^{-1} *per* added electron, Table 3.

In view of the chemical stability of the different oxidation states $[Pt_{24}(CO)_{30}]^{n-}$, we carried out an electron paramagnetic resonance (EPR) investigation of the electrogenerated monoanion $[Pt_{24}(CO)_{30}]^{-}$. Figure 7 shows the pertinent X-band spectrum at liquid nitrogen temperature.

The lineshape analysis of the paramagnetic spectrum has been carried out in terms of the multiple derivative approach coupled with spectral simulations under the assumption of a $S = 1/2$ electron-spin Hamiltonian [18–20].

The broad glassy signal is unresolved and displays significant spectral anisotropy, the bottom peak of which is in part coupled to two spurious spikes, probably arising from traces of byproducts.

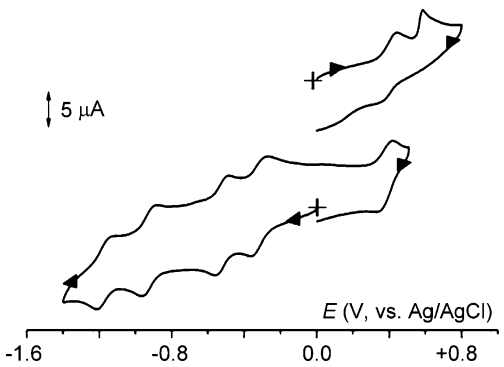

Fig. 8 Cyclic voltammetric responses recorded at a glassy carbon electrode in CH_2Cl_2 solution of $[Pt_{38}(CO)_{44}]^{2-}$ (saturated solution). $[NBu_4][PF_6]$ supporting electrolyte (0.2 mol dm^{-3}). Scan rate 0.2 V s^{-1}. T=278 K

The total lack of hyperfine (hpf) or superhyperfine (shpf) Pt-195 resolution (the so-called "wings" features) has been confirmed by a multiple-derivative approach to the experimental absorption, which in principle would arise from the effective magnetic coupling of the $S = 1/2$ unpaired electron with the Pt-195 isotopes ($I = 1/2$, natural abundance=33.7%) of the metal skeleton.

Such a spectral behaviour is conceivably assigned to the high nuclearity of the paramagnetic species and the consequent line-broadening effects, in that it often happens that the higher the nuclearity the lower the extent of hpf or shpf interactions in the presence of equivalent or near-equivalent magnetic couplings between the unpaired electron and the magnetically active metal nuclei [18–22].

On the basis of the experimental rhombic linewidth and in the absence of MO calculations, only upper limits for the underlying magnetic interactions can be proposed as $\Delta H_{exp} = 310 \pm 20\ G \geq a_i(\mathrm{Pt}-195)$.

The simulated lineshape in the first-third derivative mode [23] is consistent with the presence of three different g_i absorptions (and therefore three different linewidths ΔH_i), largely overlapping each other in the intermediate field, giving rise to the typical "rhombic" spectral symmetry [18, 19].

In this connection, Fig. 7b shows the best fit first derivative lineshape, which was achieved by assuming that the delocalization of the unpaired electron basically resides inside the multiplatinum frame and considering, at a first approach, two different sets of four magnetically coupled Pt-195 nuclei. The pertinent parameters are reported in Table 4.

Under the magnetic "spin-only" approximation, we have evaluated the corresponding μ_{eff}:

$$\mu_{\mathrm{eff}} = < g > [S(S+1)]^{1/2}$$
$$= 1.83(\pm 0.01)\ vs.\ \text{the theoretical spin}$$
$$- \text{only value of } 1.73.$$

The result well supports the basic metallic character of the unpaired spin density on the $[Pt_{24}(CO)_{30}]^{-}$

Table 5 Formal electrode potentials [V, vs. Ag/AgCl and (in brackets) vs. Fc/Fc^+] for the electron transfer processes exhibited by $[Pt_{38}(CO)_{44}]^{2-}$ in CH_2Cl_2 solution at different temperatures

Oxidation processes		Reduction processes				Temperature (K)
$E_c^{\theta,}$ (−/0)	$E_c^{\theta,}$ (2−/−)	$E_c^{\theta,}$ (2−/3−)	$E_c^{\theta,}$ (3−/4−)	$E_c^{\theta,}$ (4−/5−)	$E_c^{\theta,}$ (5−/6−)	
+0.59[a] (+0.16)[a]	+0.40 (−0.03)	−0.30 (−0.73)	−0.51 (−0.94)	−0.91 (−1.34)	−1.10 (−1.53)	278
+0.57[a] (+0.14)[a]	+0.38 (−0.05)	−0.32 (−0.75)	−0.54 (−0.97)	−0.93 (−0.36)	−1.20 (−1.63)	298
(+0.5)[b]	(+0.25)[b]	(−0.8)[b]	(−0.9)[b]	(−1.2)[b]	(−1.35)[b]	298

[a] Peak potential value for processes complicated by adsorption phenomena (see text)

[b] From [13] (approximate values from spectroelectrochemical tests)

monoanion framework (5*d* orbitals) in the presence of effective electron spin delocalization [18, 19], metallic character which is on the other hand further proved by g_i values significantly different from g=2.0023 of the "free electron".

The "orbital contribution" to the μ_{eff} can be evaluated as:

$$\left[\left(\mu_{eff} - \mu_{eff(spin-only)}\right)/\mu_{eff(spin-only)}\right] \times 100$$
$$= [(1.83 - 1.73)/1.73] \times 100 = 6\%$$

Raising the temperature, the EPR signal rapidly collapses, and at the glassy-fluid transition (187 K) it drops out, so that the fluid solution becomes EPR mute, likely because of the effective increasing of the paramagnetic relaxation rates under fast motion conditions [18, 19].

$[Pt_{38}(CO)_{44}]^{2-}$

The electrochemical behaviour of the [PPN] salt of the dianion $[Pt_{38}(CO)_{44}]^{2-}$ ($[PPN^+ = (PPh_3)_2N^+]$) is quite reminiscent of that above illustrated for $[Pt_{19}(CO)_{22}]^{4-}$ and $[Pt_{24}(CO)_{30}]^{2-}$. In fact, as shown in Fig. 8, it exhibits a pair of one-electron oxidations and two pairs of one-electron reductions, all processes exhibiting features of chemical reversibility but for the most anodic step, which, as in the previous cases, is likely affected by electrode adsorption problems of the neutral form $[Pt_{38}(CO)_{44}]^0$.

The pertinent redox potentials are compiled in Table 5.

The IR spectroelectrochemical analysis of the carbonyl frequencies accompanying the redox changes of $[Pt_{38}(CO)_{44}]^{2-}$ revealed that the species bearing an overall odd charge tend to be instable. In fact, as exemplified in Fig. 9, the one-electron reduction $[Pt_{38}(CO)_{44}]^{2-/3-}$ is in reality accompanied by the relatively fast appearance of the stretching vibration of the carbonyl group of the tetraanion $[Pt_{38}(CO)_{44}]^{4-}$, i.e. the passage $[Pt_{38}(CO)_{44}]^{2-/3-}$ does not give rise to an isosbestic point because of the fast set up of the equilibrium $[Pt_{38}(CO)_{44}]^{3-} \rightleftarrows [Pt_{38}(CO)_{44}]^{4-}$.

The carbonyl stretching vibrational frequencies of the investigated sequential electron transfers summarised in Table 6 show a perfect agreement with the previous findings [13].

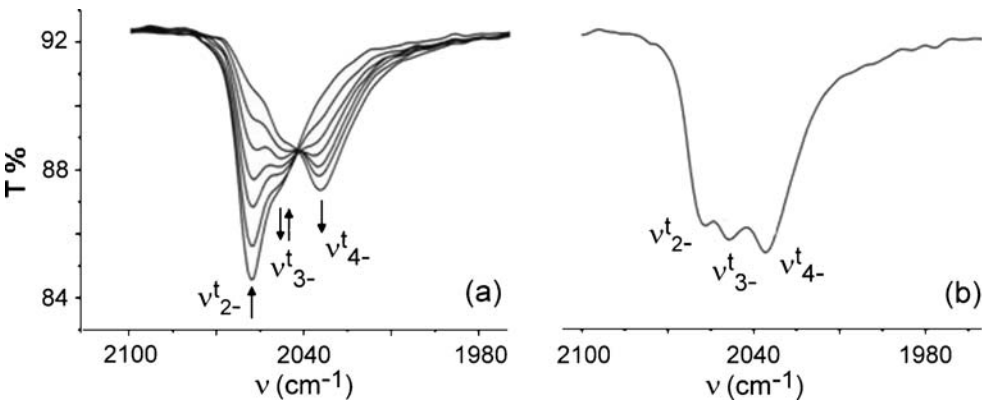

Fig. 9 IR spectral changes recorded in an OTTLE cell: **a** during the progressive reduction $[Pt_{38}(CO)_{44}]^{2-/3-}$; **b** after completion of the one-electron reduction. CH_2Cl_2 solution. $[NBu_4][PF_6]$ supporting electrolyte (0.2 mol dm^{-3})

Table 6 IR stretching frequencies of the terminal carbonyl groups (ν^t, cm^{-1}) for the series $[Pt_{38}(CO)_{44}]^{n-}$. CH_2Cl_2 solution

"*n*" cluster charge	ν^t_{CO}
2−	2,059
	2,058[a]
3−	2,048
	2,044[a]
4−	2,034
	2,033[a]
5−	2,024
	2,022[a]
6−	2,013
	2,010[a]

[a] From [13]

Conclusions

The present electrochemical and spectroelectrochemical study has confirmed, and in some cases completed, the previous investigations on the rich redox activity of the high-nuclearity platinum clusters $[Pt_{19}(CO)_{22}]^{4-}$, $[Pt_{24}(CO)_{30}]^{2-}$ and $[Pt_{38}(CO)_{44}]^{2-}$. The EPR investigation on the monoanion $[Pt_{24}(CO)_{30}]^{-}$ represents the first successful study on the paramagnetism of homoleptic platinum–carbonyl clusters.

The present study lends a perspective support to the possibility that high nuclearity platinum–carbonyl clusters might find an employment as nanocapacitors in molecular electronics.

Acknowledgement PZ and AC gratefully acknowledge the financial support from the Italian MUR (PRIN2006).

References

1. Femoni C, Iapalucci MC, Kaswalder F, Longoni G, Zacchini S (2006) Coord Chem Rev 250:1580
2. Simon U (1999) On the possibility of single electronics based on ligand-stabilized metal clusters. In: Braunstein P, Oro LA, Raithby PR (eds) Metal clusters in chemistry, vol. 3. Wiley–VCH Weinheim, pp 1342–1359
3. Schmid G, Liu YP, Schumann M, Raschke T, Radehaus C (2001) Nano Lett 1:405
4. Hoeppener S, Chi L, Fuchs H (2002) Nano Lett 2:459
5. Werts MHV, Lambert M, Bourgoin J-P, Brust M (2002) Nano Lett 2:43
6. Templeton AC, Wuelfing WP, Murray RW (2000) Acc Chem Res 33:27
7. Chi LF, Hartig M, Drechsler T, Schwaack T, Seidel C, Fuchs H, Schmid G (1998) Appl Phys Lett 66:S187
8. Carroll RL, Gorman CD (2002) Angew Chem Int Ed 41:4378
9. Sinzig J, de Jongh LJ, Cerotti A, Della Pergola R, Longoni G, Stener M, Albert K, Rosch N (1998) Phys Rev Lett 81:3211
10. Longoni G, Femoni C, Iapalucci MC, Zanello P (1999) Electron-sink features of homoleptic transition-metal carbonyl clusters. In: Braunstein P, Oro LA, Raithby PR (eds) Metal clusters in chemistry, vol. 2. Wiley, Weinheim, pp 1137–1158
11. Zanello P (1990) Stereochemical aspects of the redox propensity of homometal carbonyl clusters. In: Zanello P (ed) Stereochemistry of inorganic and organometallic compounds: chain, cluster, inclusion compounds, paramagnetic labels, and organic rings, vol. 5. Elsevier, Amsterdam, pp 163–408
12. Lewis GJ, Roth JD, Montag RA, Safford LK, Gao X, Chang SC, Dahl LF, Weaver MJ (1990) J Am Chem Soc 112:2831
13. Roth JD, Lewis GJ, Safford LK, Jiang X, Dahl LF, Weaver MJ (1992) J Am Chem Soc 114:6159
14. Washecheck DM, Wucherer EJ, Dahl LF, Ceriotti A, Longoni G, Manassero M, Sansoni M, Chini P (1979) J Am Chem Soc 101:6110
15. Ceriotti A, Masciocchi N, Macchi P, Longoni G (1999) Angew Chem Int Ed 38:3724
16. Krejčik M, Daněk M, Hartl F (1991) J Electroanal Chem 317:179
17. Zanello P (2003) Inorganic electrochemistry. Theory, practice and application. RS·C, Cambridge
18. Mabbs FE, Collison D (1992). Electron paramagnetic resonance of *d* transition metal compounds. In: Studies in inorganic chemistry, vol. 16. Elsevier, New York, pp 955-984
19. Drago RS (1992) Physical methods for chemists. Saunders College Publ., New York
20. Xiao L, Wang L (2004) J Phys Chem A 108:8605
21. Sanna G, Minghetti G, Zucca A, Pilo MI, Seeber R, Laschi F (2000) Inorg Chim Acta 305:189
22. Fabrizi de Biani F, Ienco A, Laschi F, Leoni P, Marchetti F, Marchetti L, Mealli C, Zanello P (2005) J Am Chem Soc 127:3076
23. Romanelli M (1985) Simulation Program Cu23GPN1. Department of Chemistry, University of Florence, Italy